ELSEVIER

Journal of Alloys and Compounds 230 (1995) 100–108

Journal of ALLOYS AND COMPOUNDS

The multiphase effect on crystal structure, hydrogen absorbing properties and electrode performance of Sc–Zr based Laves phase alloys

M. Yoshida[a], H. Ishibashi[a], K. Susa[a], T. Ogura[b], E. Akiba[c]

[a]*Hitachi Chemical Co., Ltd. Tsukuba Research Laboratory, 48 Wadai, Tsukuba, Ibaraki 300-42, Japan*
[b]*Shin-Kobe Electric Machinery Co. Ltd., Okabe-machi, Osato-gun, Saitama 369-02, Japan*
[c]*National Institute of Materials and Chemical Research, 1-1 Higashi, Tsukuba, Ibaraki 305, Japan*

Received 31 March 1995

Abstract

The crystal structure, hydrogen absorbing properties and electrode performance of Laves phase alloy systems, Sc–Zr–Ni–Mn and Sc–Zr–Ni–V systems, were studied by optical and scanning electron microscopy, X-ray powder diffraction, pressure–composition isotherm and electrochemical measurements. C14 and C15 Laves phases and minor ScNi-related phase were found in the Sc–Zr–Ni–Mn alloy system. The ScNi-related phase was composed of Sc, Zr and Ni elements. Two kinds of minor phase, BCC and ScNi-related phases, were identified in addition to the C15 phase in the Sc–Zr–Ni–V alloy system. The BCC contained mainly the element V. The ScNi-related phase contributed to an increase in the hydrogen capacity, but those in the V alloy system did not. The multiphase anode with a large amount of the ScNi-related phase showed a low durability against the KOH electrolyte. The substitution of Zr by Sc led to an improvement in the initial activation of the anode, but there was not a clear correlation between the presence of the multiphase in the anode and the rate capability.

Keywords: Laves phase alloy; Multiphase; Crystal structure; Hydrogen absorbing properties; Discharge capacity; Durability

1. Introduction

The nickel–hydrogen rechargeable battery (Ni–H) is one of the well known practical applications of hydrogen absorbing alloys. $LaNi_5$-related AB_5 alloys have already been commercialized [1]. Recently, the use of $ZrMn_2$-based AB_2 Laves phase alloys was intensively investigated in the field of Ni–H batteries because of their larger hydrogen absorbing capacity in comparison with $LaNi_5$ [2].

One of the present authors has investigated Sc-based Laves phase alloy electrodes and found that the Sc-based electrode with Zr substituted for Sc improved the durability and showed more than 300 mA h g^{-1} in discharge capacity at a discharge current of 70 mA g^{-1} [3].

In the case of modified or substituted AB_5 alloys, they generally exhibit a major phase with $CaCu_5$-type structure and small amounts of minor impurity phases; therefore, many efforts have been made to control the crystal structure (lattice parameter) by substitution. For example, the hydrogen plateau pressure depends exponentially on the cell volume of the alloys [4]. In the study of AB_2 Laves phase alloys, substitution is known to make a multiphase alloy depending on substituting elements and contents [5]. Therefore, in order to develop the AB_2 alloy for hydrogen storage, it is first necessary to investigate whether or not the presence of the multiphase has a good influence on the hydrogen absorbing property and for battery application.

In the previous study of the Sc-based alloys [3], the presence of the multiphase was already confirmed by X-ray diffraction, but the composition was so complicated that the phase identification was not done in detail. Thus, we selected simpler alloy systems, Sc–Zr–Ni–Mn and Sc–Zr–Ni–V, than the previous study. We made multiphase alloys and identified each phase by X-ray diffraction, optical microscopy and scanning electron microscopy. We also measured a pressure–

SSDI 0925-8388(95)01698-8

composition (PC) isotherm and took electrochemical measurements in order to study the multiphase effect on crystal structure and hydrogen and electrode performance of the Sc–Zr–Ni–Mn and Sc–Zr–Ni–V systems.

2. Experimental details

Thirteen kinds of alloy ($Sc_{1-x}Zr_xNi_{2-y}Mn_y$: $x = 0$, 0.5, 1.0, $y = 0.5$, 0.7, 0.9; $Sc_{1-x}Zr_xNi_{2-y}V_y$: $x = 0.5$, 0.7, 0.9, $y = 0.3$, 0.5, 0.7) were prepared by arc melting from 99.9% pure metals in argon atmosphere. Homogeneous samples were obtained by turning out and re-melting the alloys four times. It is very important for synthesis that the alloy on the water-cooling plate in the arc melted furnace is turned out as quickly as possible, and re-melted before it cools, otherwise it will be broken, because an intermetallic compound that is usually brittle is quite easily broken during cooling.

X-ray powder diffraction data of all the alloys were measured on a RIGAKU RAD-A diffractometer with Cu Kα radiation. The diffraction profiles were analyzed by the Rietveld method using RIETANsoftware [6]. Metallurgical examination was performed by optical microscopy and scanning electron microscopy (SEM).

The pressure–composition (PC) isotherms at 313 K were measured by a conventional constant volume apparatus [7]. Before the PC isotherm measurements all the alloys were activated by evacuating at 473 K for 3 h and by introducing hydrogen up to 5 MPa at room temperature. This treatment was repeated three times.

The electrodes were prepared by the mixture of 0.2 g alloy powder and 0.8 g Ni powder. The mixture was compacted into a pellet (10 mm diameter and 1.5 mm thickness) and then sandwiched between two sponge nickel plates ($30 \times 30 \times 1.6$ mm). Furthermore, this sandwich was compressed again for good contact. Two Ni cathodes were attached to both sides of the alloy electrode. The cathode materials were the same as those used in commercial Ni–Cd batteries and the cathode electrodes had sufficiently higher capacities than that of the anode. An electrolyte solution of 30 wt.% KOH was used. This electrochemical cell was described in detail elsewhere [8]. The electrodes were dipped into the electrolyte for 1 d, followed by the electrochemical measurement. Discharge capacities of the fully charged alloy electrodes (charge current: 70 mA g^{-1}) were measured at room temperature at 70 mA per g alloy and 490 mA per g alloy of discharge current. The cut-off voltage was 1.0 V during discharge.

3. Results

3.1. Phase analysis

C14 and C15 Laves phases and minor BCC phase were found in the Sc–Zr–Ni–Mn alloys by X-ray powder diffraction. Three kinds of the Sc–Zr–Ni–V alloy ($Sc_{0.3}Zr_{0.7}Ni_{1.3}V_{0.7}$, $Sc_{0.5}Zr_{0.5}Ni_{1.3}V_{0.7}$ and $Sc_{0.5}Zr_{0.5}Ni_{1.5}V_{0.5}$) contained two kinds of BCC phase (BCC1 and BCC2) in addition to the C15 Laves phase.

In order to identify each phase in the multiphase alloys, two typical alloys ($Sc_{0.5}Zr_{0.5}Ni_{1.3}Mn_{0.7}$, C15 Laves phase and BCC; $Sc_{0.5}Zr_{0.5}Ni_{1.3}V_{0.7}$, C15 Laves phase, BCC1 and BCC2) were analyzed by optical microscopy and scanning electron microscopy (SEM). Fig. 1(a) shows an optical micrograph of $Sc_{0.5}Zr_{0.5}Ni_{1.3}Mn_{0.7}$. A gray colony (region A), a small amount of black colony (region B) and white matrix (region C) were classified in this graph. The X-ray diffraction patterns, however, showed only two phases, major C15 phase and minor BCC phase. They correspond from the area ratio to the white matrix and the gray colony, respectively. The X-ray diffraction did not detect any phase related to the small black colony. Fig. 1(b) shows the results of SEM and EDX analysis. Zr and Ni elements homogeneously existed over all the regions. The Mn element was distributed in the white matrix; in contrast, the intensity of Sc was strong in the gray and black colonies.

Fig. 2(a) shows an optical micrograph of

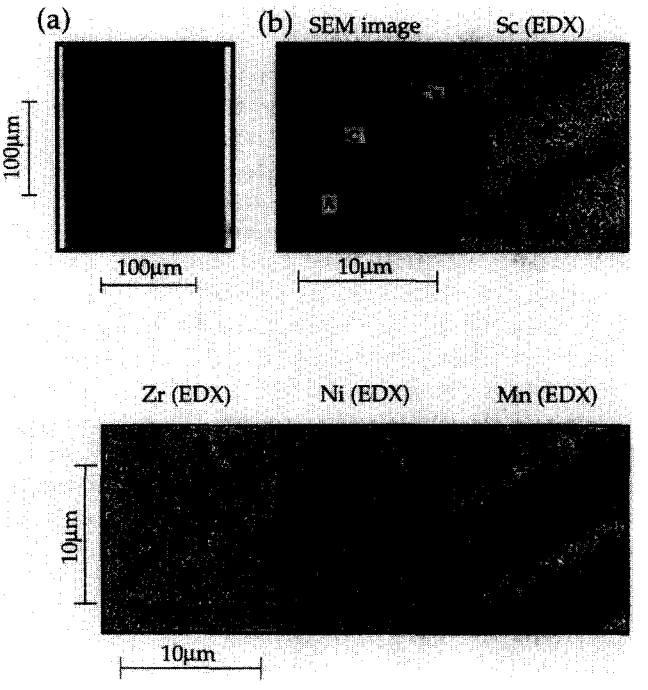

Fig. 1. (a) Optical micrograph of $Sc_{0.5}Zr_{0.5}Ni_{1.3}Mn_{0.7}$. (b) Scanning electron micrographs of $Sc_{0.5}Zr_{0.5}Ni_{1.3}Mn_{0.7}$.

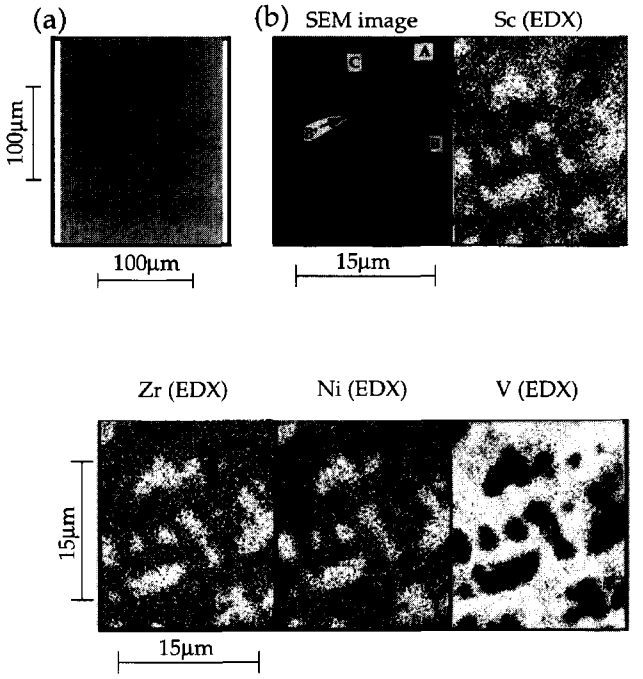

Fig. 2. (a) Optical micrograph of $Sc_{0.5}Zr_{0.5}Ni_{1.3}V_{0.7}$. (b) Scanning electron micrographs of $Sc_{0.5}Zr_{0.5}Ni_{1.3}V_{0.7}$.

$Sc_{0.5}Zr_{0.5}Ni_{1.3}V_{0.7}$. This graph contains three different regions, gray (region A) and black colonies (region B) and white matrix (region C). The SEM and EDX analysis, however, detected two kinds of black colony (small (region B′) and big ones). The big black colony mainly contained V element, and the Zr and Ni were distributed in the gray colony and white matrix as shown in the lower part of Fig. 2(b). The Sc intensity in the gray and small black colony was found to be stronger than that in the white colony. Three phases, C15 phase, BCC1 and BCC2, were identified by the X-ray diffraction in $Sc_{0.5}Zr_{0.5}Ni_{1.3}V_{0.7}$; however, no diffraction peak derived from the small black colony was detected. The lattice parameters of BCC1 and BCC2 were calculated from 2θ angle of 110 peaks to be about 3.17 and 3.00 Å, respectively. The lattice parameters of the BCC phase in the Sc–Zr–Ni–Mn alloys were close to that of BCC1. The lattice parameter of BCC2 phase was similar to that of V element ($a = 3.0274$ Å [9]); therefore the BCC2 corresponds to the black colony, and the other minor phase (BCC1) corresponds to the gray colony. The lattice parameters of the BCC in the Sc–Zr–Ni–Mn system and BCC1 containing Sc, Zr and Ni were identical to that of ScNi phase ($a = 3.171$ Å [10]); therefore it can be said that they are Zr-substituted ScNi phase (called ScNi-related phase). The BCC2 phase will be called BCC hereafter.

For Rietveld analysis of the X-ray diffraction data of the two alloys, we adopted the following model on the basis of the above metallurgical results. (1) The ScNi-related phases in the Sc–Zr–Ni–Mn and Sc–Zr–Ni–V alloys are composed of Zr, Sc and Ni, and Zr occupies Sc site of the ScNi structure [10] ($a = 3.171$ Å, $Pm\bar{3}m$, No. 219). Its chemical formula is $Sc_{0.5}Zr_{0.5}Ni$. (2) The BCC contains only V element, and has W-type structure [9] ($a = 3.0274$ Å, $Im\bar{3}m$, No. 229). (3) The chemical formula of the C15 phases of the $Sc_{0.5}Zr_{0.5}Ni_{1.3}Mn_{0.7}$ and $Sc_{0.5}Zr_{0.5}Ni_{1.3}V_{0.7}$ are $Sc_{0.5}Zr_{0.5}Ni_{1.3}Mn_{0.7}$ and $Sc_{0.5}Zr_{0.5}Ni_2$, respectively. (4) Sc and Zr occupy the A site (8d: 1/2 1/2 1/2) of the C15 phase ($Fd\bar{3}m$, No. 227), and Ni and Mn occupy the B site (16c: 1/8 1/8 1/8). Fig. 3 shows the result of Rietveld refinement for $Sc_{0.5}Zr_{0.5}Ni_{1.3}Mn_{0.7}$ that contained two phases (C15 phase: $R_I = 3.0\%$, $R_F = 2.7\%$ and BCC phase: $R_I = 3.2\%$, $R_F = 2.2\%$, S $(R_{wp}/R_e) = 1.8$). The profiles of $Sc_{0.5}Zr_{0.5}Ni_{1.3}V_{0.7}$ derived from the above model also fitted well to the measured one. The X-ray Rietveld results indicated that Sc was partially substituted by Zr in the ScNi-related phase. The phase abundance of two alloys was estimated using structure parameters obtained from Rietveld analysis. The phase abundance by weight (w_i) of each phase is given by the following equation [11];

$$w_i = \frac{(S_i \cdot D_i \cdot V_i^2)}{\sum_i (S_j \cdot D_j \cdot V_j^2)} \quad (1)$$

where S_i, D_i and V_i are the scale factor, theoretical density and volume of the ith phase, respectively. $Sc_{0.5}Zr_{0.5}Ni_{1.3}Mn_{0.7}$ was found to contain the C15 phase (81.1 wt.%) and ScNi-related phase (18.9 wt.%). $Sc_{0.5}Zr_{0.5}Ni_{1.3}V_{0.7}$ was a mixture of the C15 phase (55 wt.%), ScNi-related phase (33.1 wt.%) and BCC (11.9 wt.%). The other alloys were analyzed by the X-ray

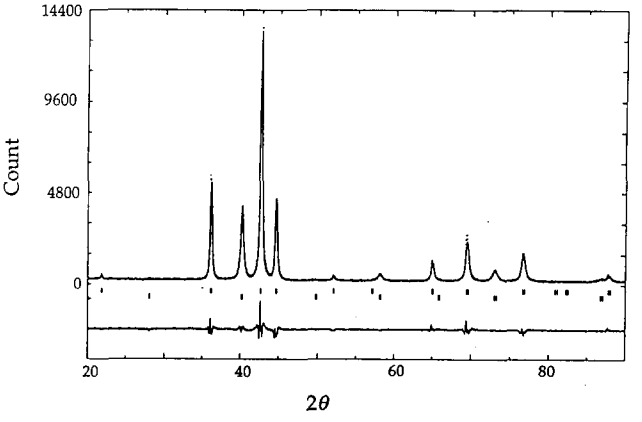

Fig. 3. Observed, calculated and difference X-ray powder diffraction patterns for $Sc_{0.5}Zr_{0.5}Ni_{1.3}Mn_{0.7}$. Upper and lower tick marks are Bragg positions for C15 Laves phase and ScNi-related phase, respectively.

Rietveld method with the above-described procedure. If the BCC phase was not contained in the Sc–Zr–Ni–V alloys, the chemical formula of the C15 phase was fixed to the nominal composition during the Rietveld refinement. Table 1 shows the results of phase abundance and lattice parameters refined by the Rietveld method for the 13 samples.

The composition of the C15 phase in $Sc_{0.5}Zr_{0.5}Ni_{1.3}Mn_{0.7}$ containing 18.9 wt.% of ScNi-related phase can be estimated to be $Sc_{0.5}Zr_{0.5}Ni_{1.4}Mn_{1.0}$, for the composition of the ScNi-related phase is assumed to be $Sc_{0.5}Zr_{0.5}Ni$. Sc and Zr are the A site elements, and Ni and Mn are the B site elements. As long as the ScNi-related phase did not contain the Mn element, the mol ratio of (Ni + Mn) to (Sc + Zr) in the C15 phase should be more than 2.0. In this case, the excess B site element (Ni or Mn) is considered to go into the A site of the AB_2; for example the formula of $AB_{2.4}$ ($Sc_{0.5}Zr_{0.5}Ni_{1.4}Mn_{1.0}$) becomes $(A_{0.88}B_{0.12})B_2$. However, to identify the composition, a closer examination by transmission electron microscopy (TEM) should be done.

Fig. 4(a) shows the results of the phase analysis in the Sc–Zr–Ni–Mn alloys. The substitution of Mn for Ni in $ScNi_2$ ($ScNi_{1.3}Mn_{0.7}$) and Sc for Zr in $ZrNi_{1.3}Mn_{0.7}$ ($Sc_{0.5}Zr_{0.5}Ni_{1.3}Mn_{0.7}$) led to the appearance of the ScNi-related phase. The ScNi phase is quite stable. When 0.5 mol of Zr was substituted for the Sc site of $ScNi_{1.3}Mn_{0.7}$, there was no significant change in the phase abundance of the ScNi-related phase. Therefore, Zr is homogeneously distributed to the ScNi-related and C15 phases. A critical composition of the C15 and C14 Laves phases existed between $Sc_{0.5}Zr_{0.5}Ni_{1.3}Mn_{0.7}$ (C15 phase) and $Sc_{0.5}Zr_{0.5}Ni_{1.1}Mn_{0.9}$ (C14 phase). It is of interest to note that the phase abundance of the ScNi-related phase drastically increased when the C14 phase appeared.

The composition of the C15 phase in $Sc_{0.5}Zr_{0.5}Ni_{1.3}V_{0.7}$ containing 33.1% ScNi-related phase (composition: $Sc_{0.5}Zr_{0.5}Ni$) and 11.9% BCC phase (V) can be estimated to be $Sc_{0.5}Zr_{0.5}Ni_{1.6}V_{0.5}$, which was different from the formula adopted in the Rietveld refinement ($Sc_{0.5}Zr_{0.5}Ni_2$). However, it is difficult to distinguish between Ni and V by X-ray diffraction because of their similar scattering power. Therefore, the difference in the chemical formula did not significantly influence the Rietveld refinement results. Fig. 4(b) shows the results of the phase analysis in the Sc–Zr–Ni–V alloys. The substitution of 0.3 mol of Sc for Zr in $ZrNi_{1.3}V_{0.7}$ or 0.7 mol of V for Ni in the $Sc_{0.3}Zr_{0.7}Ni_2$ led to the formation of small amounts of ScNi-related and BCC phases. Therefore, the appearance of those phases depends on the substituting contents of Sc and V, when $ZrNi_2$ is the base composition. Fig. 5 shows the lattice parameters of the C15 phase in $Sc_xZr_{1-x}Ni_{1.3}V_{0.7}$ ($x = 0$, 0.1, 0.3, 0.5; solid circle, C15 single phase; open circle, multiphase) and

Table 1
The results of X-ray diffraction measurements

Alloys	Phase	Lattice parameters
$ZrNi_{1.3}Mn_{0.7}$	C15(100%)	a = 7.0374(4) Å
$Sc_{0.5}Zr_{0.5}Ni_{1.1}Mn_{0.9}$	C14 (54.7%)	C14: a = 5.0151(4) Å
		c = 8.1752(6) Å,
	ScNi-related (45.3%)	ScNi-related: a = 3.1706(2) å
$Sc_{0.5}Zr_{0.5}Ni_{1.3}Mn_{0.7}$	C15 (81.1%)	C15: a = 7.0238(3) Å
	ScNi-related (18.9%)	ScNi-related: a = 3.1711(2) Å
$Sc_{0.5}Zr_{0.5}Ni_{1.5}Mn_{0.5}$	C15 (80.8%)	C15: a = 6.9880(4) Å
	ScNi-related (19.2%)	ScNi-related: a = 3.1740(2) Å
$ScNi_{1.3}Mn_{0.7}$	C15 (79.4%)	C15: a = 7.0346(3) Å
	ScNi-related (20.6%)	ScNi-related: a = 3.1572(2) Å
$ZrNi_{1.3}V_{0.7}$	C15 (100%)	a = 7.107(1) Å
$Sc_{0.1}Zr_{0.9}Ni_{1.3}V_{0.7}$	C15 (100%)	a = 7.0993(7) Å
$Sc_{0.3}Zr_{0.7}Ni_{1.3}V_{0.7}$	C15 (86.8%)	C15: a = 7.046(2) Å
	ScNi-related (5.3%)	ScNi-related:a = 3.142(2) Å
	BCC (7.9%)	BCC: a = 3.011(1) Å
$Sc_{0.3}Zr_{0.7}Ni_{1.5}V_{0.5}$	C15 (100%)	a = 7.0430(9) Å
$Sc_{0.3}Zr_{0.7}Ni_{1.7}V_{0.3}$	C15 (100%)	a = 6.9908(7) Å
$Sc_{0.5}Zr_{0.5}Ni_{1.3}V_{0.7}$	C15 (55.0%)	C15: a = 7.001(2) Å
	ScNi-related (33.1%)	ScNi-related: a = 3.176(1) Å
	BCC (11.9%)	BCC: a = 3.000(1) Å
$Sc_{0.5}Zr_{0.5}Ni_{1.5}V_{0.5}$	C15 (70.0%)	C15: a = 7.0025(7) Å
	ScNi-related (18.9%)	ScNi-related: a = 3.1841(3) Å
	BCC (11.1%)	BCC: a = 3.0018(7) Å
$Sc_{0.5}Zr_{0.5}Ni_{1.7}V_{0.3}$	C15 (87.3%)	C15: a = 6.9752(5) Å
	ScNi-related (12.7%)	ScNi-related: a = 3.1863(4) Å

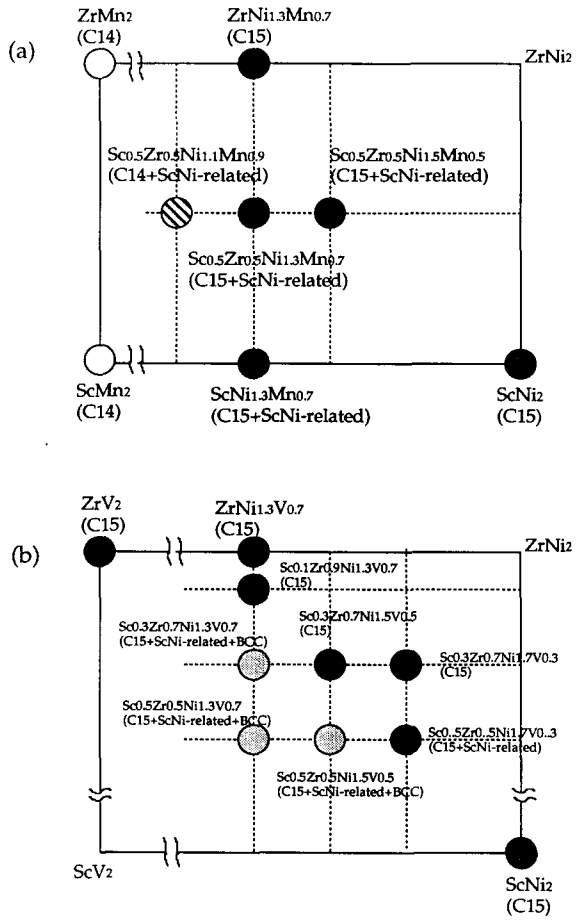

Fig. 4. (a) The result of the phase analysis in the Sc–Zr–Ni–Mn alloys. (b) The result of the phase analysis in the Sc–Zr–Ni–V alloys.

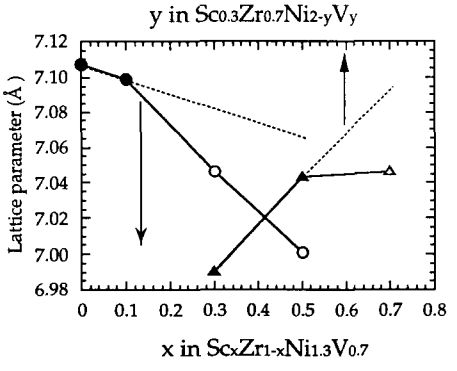

Fig. 5. The lattice parameters of the C15 phase in the $Sc_xZr_{1-x}Ni_{1.3}V_{0.7}$ ($x = 0$, 0.1, 0.3, 0.5) and $Sc_{0.3}Zr_{0.7}Ni_{2-y}V_y$ ($y = 0.3$, 0.5, 0.7). ●, $Sc_xZr_{1-x}Ni_{1.3}V_{0.7}$ ($x = 0$, 0.1: C15 single phase); ○, $Sc_xZr_{1-x}Ni_{1.3}V_{0.7}$ ($x = 0.3$, 0.5: multiphase); ▲, $Sc_{0.3}Zr_{0.7}Ni_{2-y}V_y$ ($y = 0.3$, 0.5: C15 single phase); △, $Sc_{0.3}Zr_{0.7}Ni_{1.3}V_{0.7}$ (multiphase).

$Sc_{0.3}Zr_{0.7}Ni_{2-y}V_y$ alloys ($y = 0.3$, 0.5, 0.7; solid triangle, C15; open triangle, multiphase). The substitution of Sc for Zr led to the lattice contraction of the C15 phase; in contrast, lattice expansion of the C15 phase occurred on the substitution of V for Ni, which is consistent with the result found by Züttle et. al [12]. In the previous study of Zr–Ti based Laves phase alloys [13], the lattice parameters of the C15 single phase were found to vary linearly as a function of the substituting content. In the present cases, if the other phases (ScNi-related and BCC) do not appear, the lattice parameters would have changed linearly along the dash line in Fig. 5. In the case of $Sc_{0.3}Zr_{0.7}Ni_{2-y}V_y$ alloys ($y = 0.3$, 0.5, 0.7), the lattice parameter became constant with increasing V content. The lattice parameter of $Sc_{0.3}Zr_{0.7}Ni_{1.5}V_{0.5}$ (C15 single phase) was very close to that of the C15 phase in $Sc_{0.3}Zr_{0.7}Ni_{1.3}V_{0.7}$ (C15, ScNi-related phase and BCC). That indicates the existence of a solubility limit for V element in this system in the vicinity of 0.5 mol. On the other hand, the lattice parameters of $Sc_xZr_{1-x}Ni_{1.3}V_{0.7}$ ($x = 0$, 0.1, 0.3, 0.5) continued to decrease with the increase in Sc content. It is noted that beyond $x = 0.1$ the rate of decrease became greater than the case extended linearly from the single phase region. It can be said that the lattice contraction is not only due to the increase of the Sc content in the C15 phase. The Sc content in the multiphase alloys increased with an increase in the ScNi-related phase. The composition of the C15 phase in $Sc_{0.3}Zr_{0.7}Ni_{1.3}V_{0.7}$ (C15, ScNi-related and BCC) was estimated to be $Sc_{0.5}Zr_{0.5}Ni_{1.6}V_{0.5}$. The increase of the ScNi-related phase led to a deviation from $AB_{2.0}$ stoichiometry composition, as mentioned before. If the excess B site element with a smaller radius than that of the A site element enters into the A site of AB_2, the lattice parameter would decrease. Therefore, in this case, the deviant composition from $AB_{2.0}$ and the increase in Sc content are considered to contribute to the occurrence of the lattice contraction in the C15 phase.

3.2. Pressure–composition isotherms

The PC isotherms at 313 K were measured in order to study the multiphase effect of the Sc–Zr–Ni–Mn and Sc–Zr–Ni–V alloys on the hydrogen absorbing properties, such as hydrogen capacity and hydrogen equilibrium plateau pressure. Hydrogen content was denoted by the atomic ratio of hydrogen to metal, H/M. The hydrogen capacity of each alloy was defined as the H/M determined under a hydrogen pressure of 4 MPa equilibrated at 313 K, as given in Table 2. Fig. 6(a) shows the PC isotherms of the desorption for the $Sc_xZr_{1-x}Ni_{1.3}Mn_{0.7}$ alloys ($x = 0$, 0.5, 1.0) at 313 K. Clear plateaus were observed in the isotherms of $Sc_{0.5}Zr_{0.5}Ni_{1.3}Mn_{0.7}$ and $ZrNi_{1.3}Mn_{0.7}$. The plateau pressures of the two alloys were identical. The previous study [13] of the Zr–Ti Laves phase alloys concluded that the plateau pressure of the single phase alloys is changed by the amount of substituting elements and varies exponentially with the cell volume of

Table 2
The results of PC isotherm and electrochemical measurements

Alloys	Hydrogen capacity (H/N) at 4 MPa	Discharge capacity (mA h g^{-1})	Rate capability
$ZrNi_{1.3}Mn_{0.7}$	0.89	not measured	not measured
$Sc_{0.5}Zr_{0.5}Ni_{1.1}Mn_{0.9}$	1.05	261 (70 mA g^{-1})	not measured
$Sc_{0.5}Zr_{0.5}Ni_{1.3}Mn_{0.7}$	0.96	282 (70 mA g^{-1}) 180 (490 mA g^{-1})	0.64
$Sc_{0.5}Zr_{0.5}Ni_{1.5}Mn_{0.5}$	0.67	38 (70 mA g^{-1})	not measured
$ScNi_{1.3}Mn_{0.7}$	0.98	400 (70 mA g^{-1})	not measured
$ZrNi_{1.3}V_{0.7}$	1.10	121 (70 mA g^{-1})	not measured
$Sc_{0.1}Zr_{0.9}Ni_{1.3}V_{0.7}$	1.21	300 (70 mA g^{-1})	not measured
$Sc_{0.3}Zr_{0.7}Ni_{1.3}V_{0.7}$	not measured	193 (70 mA g^{-1}) 114 (490 mA g^{-1})	0.59
$Sc_{0.3}Zr_{0.7}Ni_{1.5}V_{0.5}$	not measured	271 (70 mA g^{-1}) 163 (490 mA g^{-1})	0.60
$Sc_{0.3}Zr_{0.7}Ni_{1.7}V_{0.3}$	not measured	174 (70 mA g^{-1}) 114 (490 mA g^{-1})	0.66
$Sc_{0.5}Zr_{0.5}Ni_{1.3}V_{0.7}$	0.53	165 (70 mA g^{-1}) 90 (490 mA g^{-1})	0.55
$Sc_{0.5}Zr_{0.5}Ni_{1.5}V_{0.5}$	0.69	213 (70 mA g^{-1}) 135 (490 mA g^{-1})	0.63
$Sc_{0.5}Zr_{0.5}Ni_{1.7}V_{0.3}$	0.66	157 (70 mA g^{-1}) 106 (490 mA g^{-1})	0.68

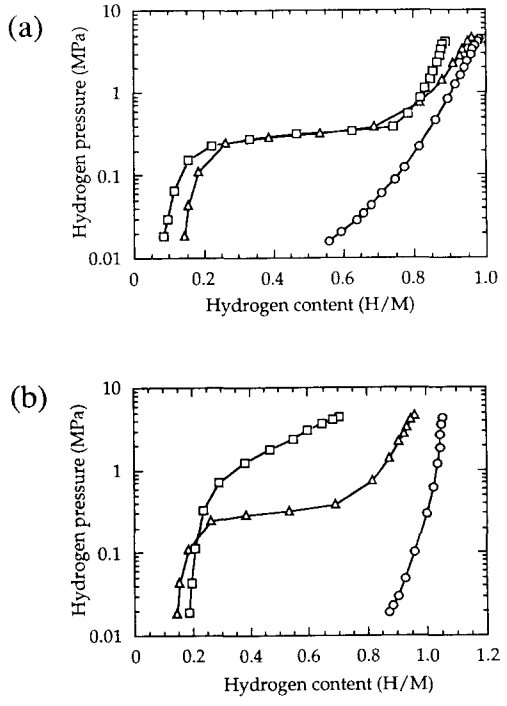

Fig. 6. (a) Pressure–composition isotherms of desorption for $Sc_xZr_{1-x}Ni_{1.3}Mn_{0.7}$ at 313 K ($x = 0$, □; 0.5, △; 1.0; ○). (b) Pressure–composition isotherms of desorption for $Sc_{0.5}Zr_{0.5}Ni_{2-y}Mn_y$ ($y =$ 0.5, □; 0.7, △; 0.9, ○).

the alloys. However, there was no correlation between the Sc content and plateau pressure in the $Sc_xZr_{1-x}Ni_{1.3}Mn_{0.7}$ alloy ($x = 0$, 0.5, 1.0) systems. Fig. 6(b) shows the PC isotherms of the desorption for the $Sc_{0.5}Zr_{0.5}Ni_{2-y}Mn_y$ alloys ($y = 0.5$, 0.7, 0.9) at 313 K. In this case, the increase of Mn content resulted in the decrease of the hydrogen equilibrium plateau pressure and the increase of the hydrogen capacity. The hydrogen capacity of $Sc_{0.5}Zr_{0.5}Ni_{1.1}Mn_{0.9}$ with the C14 phase was more than 1.0. This will probably be contributed to by the ScNi-related phase, found at up to 45.3 wt.% in this alloy. The hydrogen capacity of these alloy systems containing Mn, except for $Sc_{0.5}Zr_{0.5}Ni_{1.5}Mn_{0.5}$, was around 1.0 regardless of the number of phases and the phase abundance of the multiphase.

The PC isotherms of the Sc–Zr–Ni–V alloys were also measured at 313 K. Fig. 7 shows the results of the $Sc_{0.5}Zr_{0.5}Ni_{2-y}V_y$ ($y = 0.3$, 0.5, 0.7) alloys. No clear plateau was observed in the isotherms. The hydrogen capacities of all the alloys containing V element are listed in Table 2. It is shown in Fig. 7 that there was no clear correlation between the V content and the hydrogen absorbing properties, equilibrium plateau

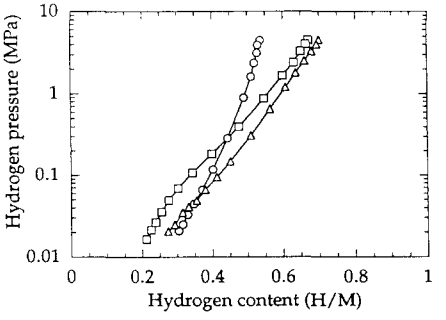

Fig. 7. Pressure–composition isotherms of desorption for $Sc_{0.5}Zr_{0.5}Ni_{2-y}V_y$ at 313 K ($y = 0.3$, □; 0.5, △; 0.7, ○).

pressure and hydrogen capacity for the multiphase alloys. However, as shown in Table 2, the C15 single phase alloys in these alloy systems were found to absorb much higher amounts of hydrogen as compared with the multiphase alloys. Therefore, the presence of multiphase was concluded to be undesirable for the hydrogen capacity.

3.3. Electrode performance

In order to investigate the multiphase effect on the electrode characteristics, electrochemical measurements of the alloys were performed at 70 and 490 mA g^{-1} of discharge currents at room temperature. The results are listed in Table 2. Fig. 8 shows discharge capacity vs. cycle number curves for the $ScNi_{1.3}Mn_{0.7}$ (C15, ScNi-related), $Sc_{0.5}Zr_{0.5}Ni_{1.3}Mn_{0.7}$ (C15, ScNi-related), $Sc_{0.5}Zr_{0.5}Ni_{1.1}Mn_{0.9}$ (C14, ScNi-related), $Sc_{0.5}Zr_{0.5}Ni_{1.3}V_{0.7}$ (C15, ScNi-related, BCC) and $Sc_{0.3}Zr_{0.7}Ni_{1.5}V_{0.5}$ (C15) anode alloys. Of all the anodes, the $ScNi_{1.3}Mn_{0.7}$ anode showed the highest discharge capacity of 400 mA h g^{-1} at the initial cycle, but the capacity rapidly decreased with increasing number of cycles. The previous study has already confirmed that this decrease was derived from the oxidation of the anode [3]. The substitution of Zr for Sc in $ScNi_{1.3}Mn_{0.7}$ increased the durability of the anode ($Sc_{0.5}Zr_{0.5}Ni_{1.3}Mn_{0.7}$) as shown in Fig. 8. However, the $Sc_{0.5}Zr_{0.5}Ni_{1.1}Mn_{0.9}$ anode containing the same amount of Zr as $Sc_{0.5}Zr_{0.5}Ni_{1.3}Mn_{0.7}$ showed a low durability, as found in the $ScNi_{1.3}Mn_{0.7}$ anode. The difference between the two anodes was the phase abundance of the ScNi-related phase ($Sc_{0.5}Zr_{0.5}Ni_{1.3}Mn_{0.7}$, 18.9 wt.%; $Sc_{0.5}Zr_{0.5}Ni_{1.1}Mn_{0.9}$, 45.3 wt.%). In the case of the $Sc_{0.5}Zr_{0.5}Ni_{1.3}V_{0.7}$ anode (ScNi-related: 33.1 wt.%, BCC: 11.9 wt.%), the discharge capacity did not decay as the cycle number increased. Therefore, one possible explanation for this is that there exists a critical amount of the ScNi-related phase for the durability of the multiphase anodes. Alternatively, the compositions of the ScNi-related phase were different; for example, the content of corrosive Sc in the ScNi-related phase of the $Sc_{0.5}Zr_{0.5}Ni_{1.1}Mn_{0.9}$ anode was greater than that of the $Sc_{0.5}Zr_{0.5}Ni_{1.3}Mn_{0.7}$.

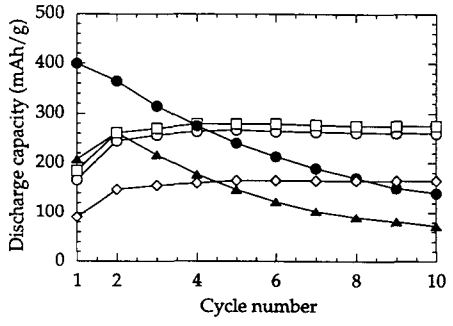

Fig. 8. Discharge capacity vs. cycle number at discharge current of 70 mA g^{-1}. ●, $ScNi_{1.3}Mn_{0.7}$; ▲, $Sc_{0.5}Zr_{0.5}Ni_{1.1}Mn_{0.9}$; □, $Sc_{0.5}Zr_{0.5}Ni_{1.3}Mn_{0.7}$; ○, $Sc_{0.3}Zr_{0.7}Ni_{1.5}V_{0.5}$; ◊, $Sc_{0.5}Zr_{0.5}Ni_{1.3}V_{0.7}$.

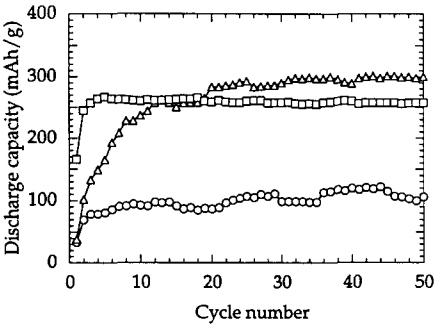

Fig. 9. Discharge capacity vs. cycle number at discharge current of 70 mA g^{-1}. ○, $ZrNi_{1.3}V_{0.7}$; △, $Sc_{0.1}Zr_{0.9}Ni_{1.3}V_{0.7}$; □, $Sc_{0.3}Zr_{0.7}Ni_{1.5}V_{0.5}$.

Fig. 9 shows the discharge capacity vs. cycle number curves of three different anodes containing C15 single phase at 70 mA g^{-1} of discharge currents. The $ZrNi_{1.3}V_{0.7}$ anode indicated a very small discharge capacity compared with that of $Sc_{0.1}Zr_{0.9}Ni_{1.3}V_{0.7}$ (300 mA h g^{-1}), in spite of their similar hydrogen absorbing capacities (see Table 2). In the case of the $Sc_{0.1}Zr_{0.9}Ni_{1.3}V_{0.7}$ anode, it took about 20 cycles to reach a constant discharge capacity. We defined the initial electrochemical activity by the number of cycles until the discharge capacity becomes saturated. The activities of $Sc_{0.1}Zr_{0.9}Ni_{1.3}V_{0.7}$ and $Sc_{0.3}Zr_{0.7}Ni_{1.5}V_{0.5}$ were 20 and 4 cycles, respectively. The $ZrNi_{1.3}V_{0.7}$ anode was not sufficiently activated at 50 cycles regardless of its high hydrogen capacity. Therefore, the substitution of Sc for Zr led to an increase in the initial electrochemical activity. The multiphase anodes having a high durability needed the same number of cycles as the $Sc_{0.3}Zr_{0.7}Ni_{1.5}V_{0.5}$ for activation. It is concluded that the distribution of Sc over the anode materials was very important for the anode to be easily activated; however, the multiphase effect on the initial activity was not clear from our present experimental results. The discharge capacity of $Sc_{0.1}Zr_{0.9}Ni_{1.3}V_{0.7}$ decreased with an increase in the discharge current. Such a trend was confirmed in both single and multiphase anodes, as seen in Table 2. The rate capability was defined by the ratio of the capacity at a current of 70 mA g^{-1} to that at 490 mA g^{-1}. When we compared the rate capabilities of the $Sc_{0.5}Zr_{0.5}Ni_{2-y}V_y$ multiphase anodes ($y = 0.3, 0.5, 0.7$), the capability decreased with the increase of the amount of the ScNi-related and BCC phases. However, there was a significant difference in the rate capability between two single phase anodes, $Sc_{0.5}Zr_{0.5}Ni_{1.5}V_{0.5}$ and $Sc_{0.5}Zr_{0.5}Ni_{1.7}V_{0.3}$. Clear correlation between the presence of the multiphase in the

anode and the rate capability was not found from our experimental results.

4. Discussion

In the single phase alloy–hydrogen systems, the following several empirical rules are generally accepted. (1) The hydrogen plateau pressure decreases with increasing cell volume [4]. (2) The lattice parameter can be controlled by substituting elements with different atomic radius. (3) The lower the equilibrium plateau pressure, the higher is the amount of hydrogen absorbed [13], because the hydrogen capacity is dependent on the hydrogen pressure at which the capacity is defined. Therefore, the alloys with a large crystal lattice have a high hydrogen capacity. However, over the mixture region of the single phase and the multiphase, there was no correlation between the substituting content and these properties, lattice parameter, hydrogen plateau pressure, from our experimental results. For example, the plateau pressure of $ZrNi_{1.3}Mn_{0.7}$ (C15 single phase) was identical to that of $Sc_{0.5}Zr_{0.5}Ni_{1.3}Mn_{0.7}$ (C15 and ScNi-related phase) which was substituted by 0.5 mol of Sc on Zr site of the $ZrNi_{1.3}Mn_{0.7}$. Furthermore, in the multiphase $Sc_{0.5}Zr_{0.5}Ni_{2-y}V_y$ ($y = 0.3$, 0.5, 0.7) alloys containing different amounts of the component phases, it was found that the hydrogen absorbing properties cannot be controlled by the V-substituting content, as shown in Fig. 7. This is because the PC isotherm of the multiphase alloy was derived from the combination of that of each constituent phase. It is very important for the multiphase alloy–hydrogen systems to focus on the hydrogen absorbing properties of each phase. In the Sc–Zr–Ni–Mn alloys, $ScNi_{1.3}Mn_{0.7}$, $Sc_{0.5}Zr_{0.5}Ni_{1.3}Mn_{0.7}$ and $Sc_{0.5}Zr_{0.5}Ni_{1.5}Mn_{0.5}$ containing similar amounts of the C15 and ScNi-related phases were compared with regard to the lattice parameter, hydrogen capacity and plateau pressure. Fig. 10 shows their PC isotherms (desorption) at 313 K. The lattice parameters of their C15 phase and the hydrogen capacity increased in the order $Sc_{0.5}Zr_{0.5}Ni_{1.5}Mn_{0.5} < Sc_{0.5}Zr_{0.5}Ni_{1.3}Mn_{0.7} < ScNi_{1.3}Mn_{0.7}$. The plateau in the PC isotherms of $Sc_{0.5}Zr_{0.5}Ni_{1.5}Mn_{0.5}$–$H_2$ was not clear within the present experimental limits; however, from the curves in Fig. 10 its plateau pressure can be judged to be higher than that of the $Sc_{0.5}Zr_{0.5}Ni_{1.3}Mn_{0.7}$–$H_2$ system. In the case of the $ScNi_{1.3}Mn_{0.7}$–H_2 system, no plateau was observed in the PC isotherm. The plateau pressure of the $ScNi_{1.3}Mn_{0.7}$–H_2 system seems to be very low. Therefore, the plateau pressure decreased in the order $Sc_{0.5}Zr_{0.5}Ni_{1.5}Mn_{0.5} < Sc_{0.5}Zr_{0.5}Ni_{1.3}Mn_{0.7} < ScNi_{1.3}Mn_{0.7}$. Since the phase abundance of the minor ScNi-related phase in the three alloys was almost identical (19–21 wt.%), the plateau pressure of these multiphase alloy systems should be determined by that of the C15 major phase. In this case, it was found that the lattice parameter of the C15 increases with a decrease of the plateau pressure and with an increase of the hydrogen capacity.

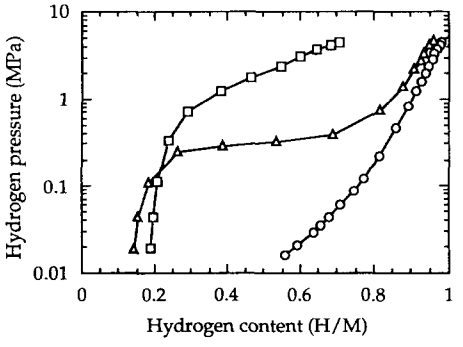

Fig. 10. Pressure–composition isotherms of desorption for the Sc–Zr–Ni–Mn alloy systems containing similar phase abundance of ScNi-related phase at 313 K. □, $Sc_{0.5}Zr_{0.5}Ni_{1.5}Mn_{0.5}$; ScNi-related: 19.2 wt.%, C15: $a = 6.9880$ Å. △, $Sc_{0.5}Zr_{0.5}Ni_{1.3}Mn_{0.7}$; ScNi-related: 18.9 wt.%, C15: $a = 7.0238$ Å. ○, $ScNi_{1.3}Mn_{0.7}$; ScNi-related: 20.6 wt.%, C15: $a = 7.0346$ Å.

In the multiphase alloys with similar phase abundance, there exists a correlation between the lattice parameter and the hydrogen absorbing properties of the major phase. When the multiphase alloys have different phase abundance, it is necessary to establish the method for estimating the hydrogen absorbing property of the multiphase alloys from that of each phase. Iba et al. [5] has reported that the hydrogen capacity, which is one of the hydrogen absorbing properties, is expressed by a linear combination for the Zr–Ti–Mn–V alloy system. For example, if the alloy A is composed of B phase and C phase, the hydrogen capacity of the alloy A is expressed by the following equation;

$$X_A = \alpha X_B + \beta X_C$$

where X, α and β are hydrogen capacity and weight fraction of B and C phases, respectively. By using this relation we estimated the hydrogen capacity of each phase in the two alloys containing different phase abundance, $Sc_{0.5}Zr_{0.5}Ni_{1.1}Mn_{0.9}$ (ScNi-related, 45.3 wt.%; C14, 54.7 wt.%) and $Sc_{0.5}Zr_{0.5}Ni_{1.5}Mn_{0.5}$ (ScNi-related, 19.2 wt.%; C15, 80.8 wt.%). In the case of $Sc_{0.5}Zr_{0.5}Ni_{1.1}Mn_{0.9}$, its total hydrogen capacity was 1.05. A typical C14 phase alloy, $ZrMn_2$, absorbs hydrogen up to a H/M value of nearly 1.0 [14]. Thus, when the hydrogen capacity of the C14 phase in this alloy is assumed to be 1.0, the ScNi-related phase is to absorb hydrogen up to about 1.1 under 4 MPa of hydrogen at 313 K. It can be said that the ScNi-related

phase contributes to raising the hydrogen absorbing capacity and that its capacity is similar to that of the C14 phase in the present study. $Sc_{0.5}Zr_{0.5}Ni_{1.5}Mn_{0.5}$ absorbed hydrogen up to an H/M of 0.67, which is two-thirds of the hydrogen capacity of the other alloys containing Mn. The hydrogen capacity of the C15 phase in this alloy can be calculated by using a linear combination to be about 0.57 with an assumption that the hydrogen capacity of the ScNi-related phase is 1.1.

Consequently, in the AB_2 multiphase alloy system, the substituting effect on the hydrogen absorbing properties is not simple as compared with the AB_2 single phase alloy systems.

5. Conclusion

We studied the multiphase effect on the crystal structure, hydrogen absorbing properties and electrode performance of the Laves phase alloy systems, Sc–Zr–Ni–Mn, and Sc–Zr–Ni–V.

(1) C14, C15 Laves phases and a minor ScNi-related phase were found in the Sc–Zr–Ni–Mn alloys. The ScNi-related phase was composed of Sc, Zr and Ni elements. The ScNi-related phase and BCC appeared in addition to the C15 Laves phase in the Sc–Zr–Ni–V alloys. The BCC mainly consisted of V element.

(2) There is no clear correlation between the amount of substituting elements and hydrogen absorbing properties (equilibrium plateau pressure and hydrogen capacity) in the multiphase alloy systems. The ScNi-related phase contributed to the high hydrogen capacity. The presence of the multiphase does not seem to have a good influence on the hydrogen capacity in the Sc–Zr–Ni–V alloys.

(3) The anode material with a large amount of the ScNi-related phase showed a low durability against the KOH electrolyte. The Sc element played an important role in the improvement of the initial activation, but there was not a clear correlation between the multiphase and the rate capability.

Acknowledgements

We thank Mr. Y. Ishido of Shin-Kobe Electric Machinery Co., Ltd. and Mr. K. Nomura of the National Institute of Materials and Chemical Research for technical assistance.

References

[1] G. Sandrock, S. Suda and L. Schlapbach, in L. Schlapbach (ed.), *Hydrogen in Intermetallic Compounds II*, Springer-Verlag, 1992, p. 197.
[2] S. Fujitani, I. Yonezu, T. Saito, N. Furukawa, E. Akiba, H. Hayakawa and S. Ono, *J. Less-Common Met., 172–174* (1991) 220.
[3] M. Yoshida, H. Ishibashi, K. Susa, T. Ogura and E. Akiba, *J. Alloys Comp., 226* (1995) 161.
[4] M.H. Mendelsohn, D.M. Gruen and A.E. Dwight, *Nature, 269* (1977) 45.
[5] H. Iba and E. Akiba, *J. Japan Inst. Metals, 58* (1994) 1225.
[6] F. Izumi, in R.A. Young (ed.), *The Rietveld Method*, Oxford University Press, Oxford, 1993, Chapter 13.
[7] K. Nomura, H. Uruno, S. Ono, H. Shinozuka and S. Suda, *J. Less-Common Met., 107* (1985) 221.
[8] J. Huot, E. Akiba, T. Ogura and Y. Ishido, *Denki Kagaku, 61* (1993) 1424; J. Huot, E. Akiba, T. Ogura and Y. Ishido, *J. Alloys Comp., 218* (1995) 101.
[9] P. Villars and L.D. Calvert, *Pearson's Handbook of Crystallographic Data for Intermetallic Phases*, Vol. 4, ASM international, Materials Park, 1993, p. 5353.
[10] P. Villars and L.D. Calvert, *Pearson's Handbook of Crystallographic Data for Intermetallic Phases*, Vol. 4, ASM international, Materials Park, 1993, p. 4670.
[11] R.J. Hill, *Powder diffraction, 6* (1991) 74.
[12] A. Züttel, F. Meli and L. Schlapbach, *J. Alloys Comp., 203* (1994) 235.
[13] M. Yoshida and E. Akiba, *J. Alloys Comp., 224* (1995) 121.
[14] J.-J. Didisheim, K. Yvon, D. Shaltiel and P. Fischer, *Solid State Commun., 31* (1979) 47.